AD-A063 264 NAVAL RESEARCH LAB WASHINGTON D C F/G 9/3
PHOTOCONDUCTIVE CONTROL OF MICROWAVES.(U)
SEP 78 A P DEFONZO
UNCLASSIFIED NRL-8239 NL

| OF |
AD
A063264

END
DATE
FILMED
3--79
DDC

LEVEL II

NRL Report 8239

Photoconductive Control of Microwaves

ALFRED P. DeFONZO

Optical Techniques Branch
Optical Sciences Division

September 21, 1978

NAVAL RESEARCH LABORATORY
Washington, D.C.

SECURITY CLASSIFICATION OF THIS PAGE *(When Data Entered)*

REPORT DOCUMENTATION PAGE

READ INSTRUCTIONS BEFORE COMPLETING FORM

1. REPORT NUMBER: NRL Report 8239
2. GOVT ACCESSION NO.:
3. RECIPIENT'S CATALOG NUMBER:

4. TITLE *(and Subtitle)*: PHOTOCONDUCTIVE CONTROL OF MICROWAVES

5. TYPE OF REPORT & PERIOD COVERED: Interim report on one phase of a ~~continuing NRL~~ problem

6. PERFORMING ORG. REPORT NUMBER:

7. AUTHOR(s): Alfred P. DeFonzo

8. CONTRACT OR GRANT NUMBER(s):

9. PERFORMING ORGANIZATION NAME AND ADDRESS:

10. PROGRAM ELEMENT, PROJECT, TASK AREA & WORK UNIT NUMBERS: NRL Problems N01-70 and P01-17 (DARPA) DARPA Order 3212

11. CONTROLLING OFFICE NAME AND ADDRESS: Department of the Navy, Office of Naval Research, Arlington, VA 22217

12. REPORT DATE: September 21, 1978

13. NUMBER OF PAGES: 28

14. MONITORING AGENCY NAME & ADDRESS *(if different from Controlling Office)*: NRL-8239

15. SECURITY CLASS. *(of this report)*: Unclassified

15a. DECLASSIFICATION/DOWNGRADING SCHEDULE:

16. DISTRIBUTION STATEMENT *(of this Report)*

Approved for public release; distribution unlimited. 21 Sep 78

17. DISTRIBUTION STATEMENT *(of the abstract entered in Block 20, if different from Report)*

28 p.

18. SUPPLEMENTARY NOTES

19. KEY WORDS *(Continue on reverse side if necessary and identify by block number)*

Microwaves
Optoelectronic devices
Phase shifters
Photoconductivity
Semiconductor plasma

20. ABSTRACT *(Continue on reverse side if necessary and identify by block number)*

A phenomenological model of microstrip semiconductor modulators has been developed. The fundamental limitations on the device imposed by the photoconductive process were expressed in terms of the product of gain and bandwidth. Based on this analysis, an optical gap modulator was fabricated and tested. Its performance approached the fundamental limit imposed by the saturation of photoconductive carrier densities resulting from Auger processes. Drift mobility in the space-charge-limited region was measured and the surface mobility of holes in silicon was determined to be 160(sq cm/V-s). It was found that annealing induced photosensitivity in silicon, and associated charges in the dark I–V characteristics are consistent with the Mott–Gurney law.

DD FORM 1 JAN 73 1473 EDITION OF 1 NOV 65 IS OBSOLETE
S/N 0102-014-6601

251 950

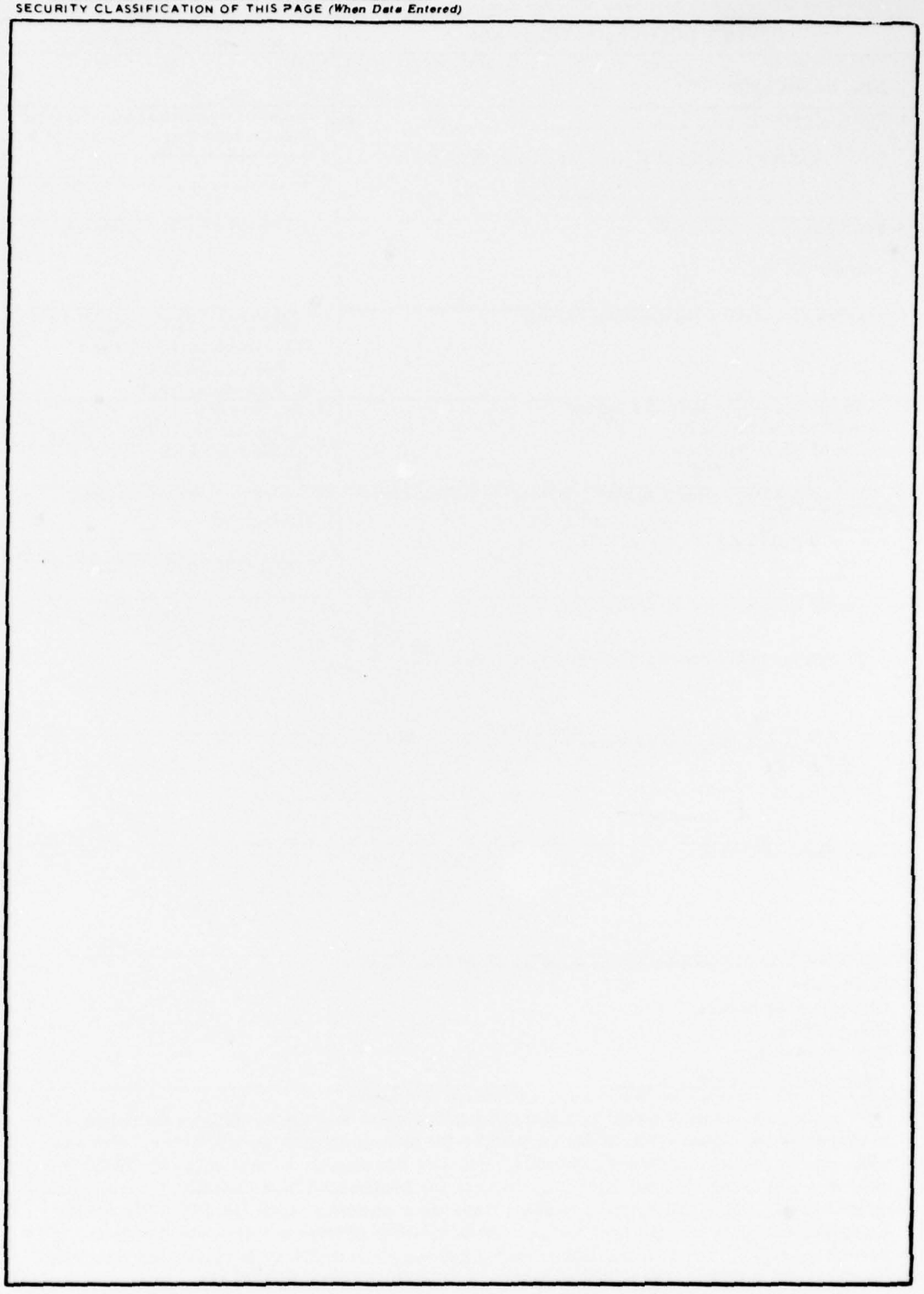

CONTENTS

INTRODUCTION 1

BASIC DEVICE 2

Practical Limitations 8
Gallium Arsenide Switch 10
Clippers 12
Modulators 12

MODULATORS 13

Fundamental Parameters 14
Gain—Bandwidth Limitations 17

CONCLUSIONS 19

REFERENCES 19

APPENDIX — The Microstrip Switch Characteristics 21

PHOTOCONDUCTIVE CONTROL OF MICROWAVES

INTRODUCTION

Photomodulation of semiconductor electrical properties takes on a new and increasing significance in the context of rapidly developing optical and microwave technology. In the past, photogenerated pairs of electron holes in semiconductors have served as the basis for many well-known applications, the more obvious being detectors and high-isolation amplifiers. Injection of light into the active regions of semiconductor devices has been successful in achieving highly isolated triggering of high-power bistable switches (light-activated silicon-controlled rectifiers (LASCR)) and in stabilizing the operation of microwave devices (Trapatts). More recently, ultrafast electrical pulse generation and switching were achieved by direct optical modulation of the transmission properties of microstrip waveguiding media. The evaluation of this latest development is the subject of this report.

Microstrip is emerging as a promising technology for manipulating microwave signals well into the gigahertz regime. It is compact and lightweight, and has relatively low loss and dispersion. Fabrication on a high-resistivity semiconductor substrate allows significant modulation of its impedance by optical injection of free carriers. The simplest embodiment of this concept is illustrated in Fig. 1. Carriers injected into the bulk of the semiconductor reduce the impedance to the grounding plane, causing an impedance mismatch that modulates the output of an applied bias at the output terminal. In 1974 Auston [1] first recognized, demonstrated, and extended this simple concept by incorporating gap into the microstrip and alternately injecting carriers across the gap and through the base. With a DC bias and a sequence of two ultrashort light pulses, Auston was able to generate extremely short electrical pulses (< 50 ps) at amplitudes exceeding 1 kV into a 50-Ω line. In a similar fashion he was also able to generate an extremely short burst of microwave signals (1 cycle at 1 GHz). (See Fig. 2.)

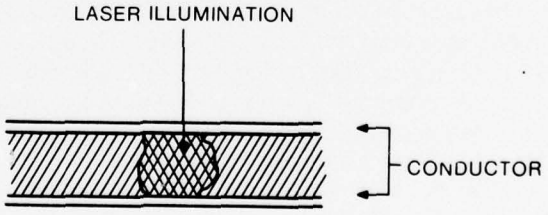

Fig. 1 — Impedance modulation by optical injection of free carriers in the semiconductor slab

Manuscript submitted June 7, 1978.

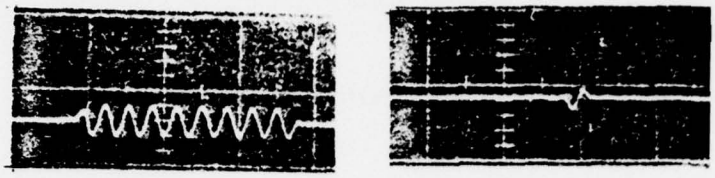

(a) (b)

Fig. 2 — Gating of a 1-GHz signal. The delay between the infrared and green pulses was approximately 8 ns in (a) and 1 ns in (b). (3 ns/div)

This generation of short bursts of microwave- and millimeter-wave signals at relatively high powers (1 kW) was a promising advance in the state of the art for high-speed switching. The fastest PIN diodes have much slower switching speeds (> 1 ns) and power handling (10 W) capabilities. Being in its early stage of development, the true potential of photoconductive microstrip switches is not clear.

Apparent advantages are the nearly infinite isolation between the light source and microwave source, a rise time limited by the optical pulse, and an instantaneous electrical bandwidth that can approach hundreds of gigahertz. Apparent disadvantages are (a) the necessity for two high-powered, short, optical pulses, each at a different wavelength, (b) the low isolation across the gap prior to optical injection, and (c) the lingering conductivity of electron-hole pairs. Not apparent are the full implications of these advantages and disadvantages. There is then a dual purpose of this report. On one level, it addresses these obvious disadvantages to determine whether engineering solutions exist. On another, it seeks to understand the true nature of the device and its fundamental limitations.

The report is divided into two sections. In the first section we report on the basic device, new configurations, and fabrication techniques. In the second section we report on methods of modeling the device, an evaluation of factors affecting performance, and improvements in the basic operating characteristics.

BASIC DEVICE

The basic switch, first introduced by Auston, as shown in Fig. 3, consists of an aluminum microstrip deposited on a high-resistivity ($\rho = 10^4$ Ω-cm) silicon substrate. The active region of the device is a small gap of length ℓ in the aluminum strip. The characteristic impedance Z_0 of the microstrip line up to the active region is determined by the dielectric constant of the substrate and the ratio (W/h) of the strip width W to the substrate thickness h. For a 50-Ω line on silicon ($\epsilon_r = 11.8$), this ratio is 0.8. The other parameters that characterize the strip are the attenuation constant α, the quality factor Q, and the cut-off frequency f_c. Microstrip may be approximated as a transverse electromagnetic (TEM) device, but this approximation breaks down at higher frequencies and for high-impedance lines. It has relatively low dispersion away from the cut-off frequency. These parameters may be determined to a good approximation by the methods described in Schneider [2].

Fig. 3 — Basic switch configuration

A picture of a typical gap device that we have fabricated at the Naval Research Laboratory is shown in Fig. 4. It has the parameters given in Table 1.

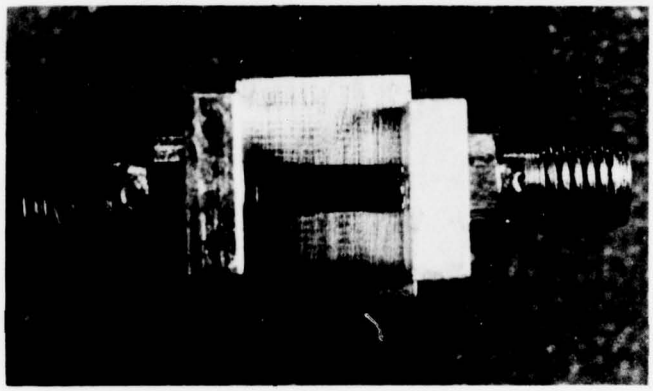

Fig. 4 — Silicon switch with a 30-mil gap mounted on an aluminum block

The equivalent circuit is shown in Fig. 5. We may analyze this network using the ABCD matrices [3] to obtain the following for the gap transmission:

$$\begin{vmatrix} A & B \\ C & D \end{vmatrix} = \begin{vmatrix} 1 & \frac{1}{Y_g} \\ 0 & 1 \end{vmatrix}, \tag{1}$$

from which we have

$$\alpha = 20 \log \left| \frac{1}{S_{21}} \right| = 10 \log \frac{1}{4} \left| 2 + \frac{1}{Y_g Z_0} \right|^2 = 10 \log \frac{1}{T}, \tag{2}$$

where

$$T = 4\left(\frac{1}{\left(2 + \frac{1}{Y_g Z_0}\right)^2}\right), \tag{3}$$

$$T_{\text{open}} = \frac{4[Z_0{}^2 G^2 + (\omega C_g Z)^2]}{(2GZ_0 + 1)^2 + (2\omega C_g Z_0)^2} \tag{4}$$

Table 1 — Parameters of a Typical Gap Device Fabricated at NRL

Parameter	Substrate	Stripline	Gap
Material	π-silicon $N_A - N_D = 10^{12}$ cm^{-3} $\rho = 3 \times 10^4 \Omega$-cm	Aluminum	
Thickness	$h = 0.025$ cm	$t = 5000$ Å	
Width	0.25 cm	$w = 0.02$ cm	$w = 0.02$ cm
Length	1 cm		$\ell = 0.038$ cm
Characteristic impedance	$Z_0 = 50\Omega$		
Gain factor	$Q_0 = 0.23$	(at 1 GHz)	
Insertion loss	$\alpha_0 = 3$ dB/cm	(at 1 GHz)	
Cut-off frequency	$f_c = 90$ GHz		

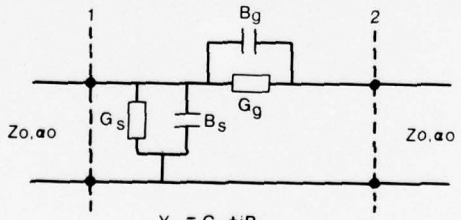

$Y_g = G_g + iB_g$

G_g = DARK CONDUCTANCE

G_s = DARK CONDUCTANCE

Fig. 5 — Equivalent circuit for the active region of a simple gap switch

where α is the attenuation across the gap, T the transmission across the gap, Z_0 the characteristic impedance of the microstrip line, and Y_g the gap admittance. This relation yields the prediction of the basic transmission properties of the switch.

Similarly, for the shunting component of the admittance Y_s, assuming that $G_1 >> \omega C_g$ and $G_2 >> \omega C_s$, we have

$$\begin{vmatrix} A & B \\ C & D \end{vmatrix} = \begin{vmatrix} 1 & 0 \\ G_2 & 1 \end{vmatrix} \begin{vmatrix} 1 & \frac{1}{G} \\ 0 & 1 \end{vmatrix}, \tag{5}$$

so that

$$T = \left(\frac{2G_1 Z_0}{1 + 2G_1 Z_0 + G_2 Z_0 + G_1 G_2 Z_0{}^2} \right)^2 , \tag{6}$$

where G_1 is the photoconductance of the gap and G_2 is the photoconductance to the ground plane. If the bulk lifetime of a photoexcited carrier is assumed to be greater than the transit time, the contacts are ohmic, and if the effective mass approximation is valid, then the expression for the conductances G_1 and G_2 is

$$G_1 = \frac{4n_r}{(n_r + 1)^2} \left(\frac{e}{\hbar\omega} \right) (\mu_n + \mu_p) \frac{\epsilon_1}{\ell^2} , \tag{7}$$

where

n_r = refractive index of the substrate
$\hbar\omega/e$ = photon energy in volts
$\mu_n + \mu_p$ = sum of electron and hole mobilities
ϵ_1 = energy of green pulse on the gap.

Similarly, one can obtain an approximate expression for the shunt conductance G_2:

$$G_2 \cong \frac{2\alpha_2}{\hbar} \frac{e}{h\omega} (\mu_n + \mu_p)\epsilon_2, \; \alpha_2 h \ll 1 \tag{8}$$

where

α_2 = absorption constant at 1.06 μm in silicon
h = substrate thickness
ϵ_2 = 1.06-μm pulse energy incident on gap
$\hbar$ = Planck's constant normalized by 2π.

For a switch whose characteristics are given in Table 1, Eqs. (7) and (8) predict the normalized conductances

$$G_1 Z_0 = 18/\mu J \tag{9}$$

and

$$G_2 Z_0 = 12/\mu J \ . \tag{10}$$

We examined the performance of a switch whose characteristics are given in Table 1. The aluminum stripline was evaporated through a bimetallic mask to a depth of 5000 Å, and then heat treated for 10 min in a 15% hydrogen, 85% nitrogen atmosphere at 500°C (see Appendix).

In Fig. 6 we show the experimental configuration used to test the microstrip in a DC switching mode. The coaxial line leading to the switch was charged typically to 20 V, and the optically induced transient was recorded on a wide-bandwidth oscilloscope. Generation of this transient requires that the amplified, single-pulse output at both the fundamental (1.06 μm) and second harmonic (0.53 μm) of a passively mode-locked Nd:YAG laser be focused on the gap in the microstrip.

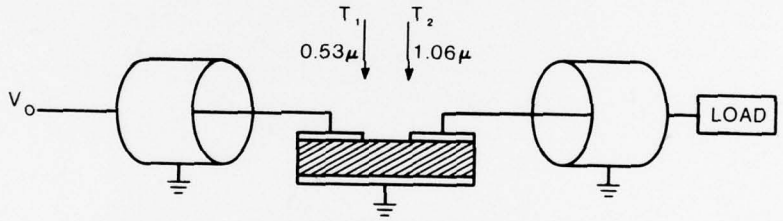

Fig. 6 — Experimental configuration of microstrip in DC and AC switching modes

In Fig. 7 we show the switching obtained for a bias of 20 V/DC, a delay between pulses of 3.5 ns, and an energy of 1 μJ at 0.53 μm and 5 μJ at 1.06 μm. Our results confirm the feasibility of DC switching [1]. Two qualifications must be added. First, the overall performance of the switch in this mode is far more sensitive to geometry and preparation techniques than Eqs. (1) through (10) suggest. Second, the values of the mobility we would need to get good agreement with theory differ significantly from the bulk values.

If one assumes bulk mobilities, these switches require laser energy at 0.53 μm, greater by an order of magnitude, to achieve the theoretically predicted transmission in the "on" state. Thus, more carriers are needed to achieve efficient switching than were predicted.

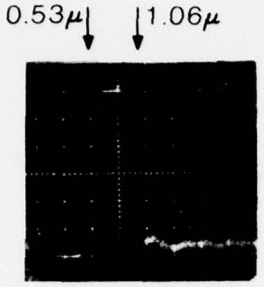

Fig. 7a — DC switching. A bias +20 V is applied to the switch. The 106-μm pulse is delayed 3.5 ns with respect to the 0.53-μm pulse.

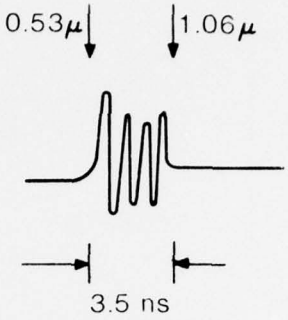

Fig. 7b — AC switching. A 1-GHz signal is applied to the switch.

We will return to these deviations in the section on modulators. As an intuitive guide, it should be kept in mind that the average current passing through the switch in any given time interval is proportional to the product of the average number of carriers in the photoconduction and the average contribution per carrier. The dynamics of carriers in this configuration are extremely complicated and do not lend themselves to analysis. Nevertheless, we expect the instantaneous transmission at the time of the "on" pulse to approach that predicted by Eqs. (7) and (4), with deviations resulting primarily from electron—electron interactions as the density increases.

The AC transmission of the switch is demonstrated in Fig. 7b. With a laser energy of 1.0 μJ at 0.53 μm and 10 μJ at 1.06 μm, and a bias signal at 1 GHz of 1.5 mW, we obtain $T_{on} = 90\%$, $T_{off} = 5.0\%$.

Up to the present time, the above concept has been utilized primarily for switching. There are two other possible applications for this approach. The first possibility is the optically controlled modulation of microwaves, switching being a limiting case. We will discuss this in greater detail later in this section. The second possibility is phase shifting. We have demonstrated this for the first time. Figure 8 shows the experimental setup. A reflection phase shifter is constructed by incorporating a 50-Ω microstrip line without a gap into a length of 50-Ω coaxial cable terminated by a short. Illuminating the switch with a single pulse of 1.06 μm radiation shorts the strip to ground, and a phase shift

$$\Delta\phi = \frac{2\pi\Delta\ell}{\lambda} \tag{11}$$

results. Utilizing a simple normally null bridge constructed of coaxial line, we detected the phase shift by a deviation from the null point that occurred after laser illumination.

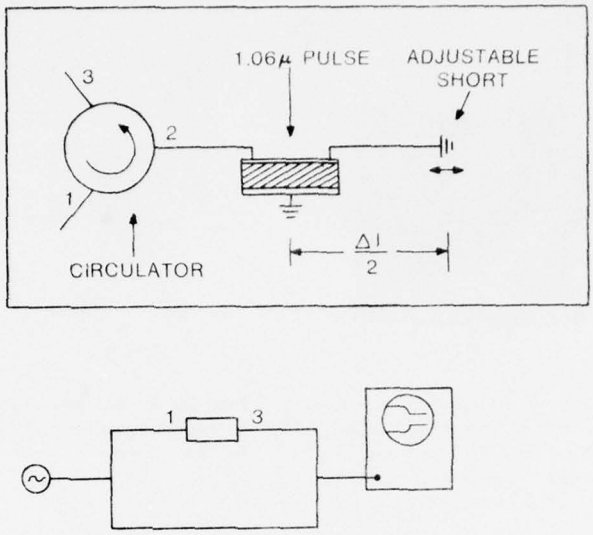

Fig. 8 — Setup for phase shift measurements

As shown in Fig. 9a, an imbalance in the bridge can be caused by either a change in attenuation or phase in an arm. To examine the relative effect of attenuation and phase shift, we examined the transmission of the phase shifter as a function of time after illumination by removing the balancing signal from the bridge. The results are shown in Fig. 9b. Initially, the plasma is highly conducting and most of the microwave signal (60%) is reflected into the output port of the circulator. As the plasma decays, the magnitude of the reflected signal at the injection point decreases. The transmitted signal is initially attenuated by the plasma. After approximately 6 μs, no signal power is reflected from the plasma (≈0%) and no power is transmitted (≈0%) through to the short and back again to the circulator, all the power being absorbed in the plasma. This gives rise to the null point. As the density of the plasma further decreases, its reflection continues to be zero, but the absorption decreases so that the net transmission after reflection from the adjustable short increases, approaching 100% as the few remaining carriers recombine.

Practical Limitations

The basic operating characteristics of the Auston switch have been confirmed and the extension of the concept to phase shifting demonstrated. Practical limitations that have appeared are as follows:

1. Two light signals — at two different wavelengths — are needed to complete a switching cycle.

2. Carrier lifetime — the persistence of carriers long after the switching event — creates spurious signals and low isolation, and decreases the optical modulation bandwidth.

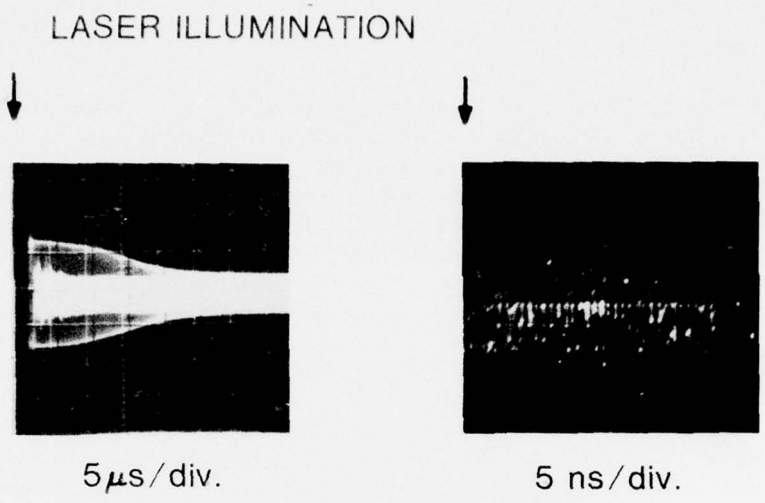

Fig. 9a — Optically generated phase shift in a normally null bridge

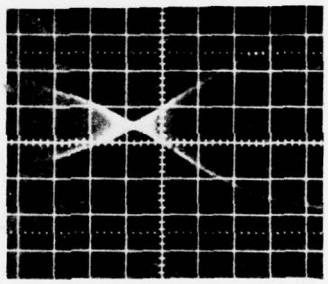

Fig. 9b — Transmission of phase shifter after optical illumination

3. High levels of injection, for ultrafast switching achieving the high density plasmas (10^{20} cm^{-3}) necessary for efficient switching with reasonable isolation and power-handling capabilities, require substantial laser energies. For picosecond switching, the laser is typically delivering the order of 1 MW across an area of the order of 10^{-4} cm^2.

4. High-resistivity silicon — the resistivity of silicon is relatively low even in the purest of specimens ($10^4 \Omega$-cm). As a result, the stripline is lossy and ohmic heating occurs when large biases are applied (> 50 V).

Gallium Arsenide Switch

Using gallium arsenide (GaAs) as a substrate offers several advantages. The mobility of the carriers is higher, along with the resistivity at room temperature. As a result, the change in conductivity with illumination is greater. The high resistivity allows larger voltage standoffs without excessive ohmic heating, as well as lower insertion losses. One main disadvantage is that GaAs does not absorb light at 1.06 μm, thus the switch cannot be turned on and off in the same fashion as silicon switches. There are three ways to overcome this. First, deep trapping centers may be introduced that quench the conductivity in a characteristic lifetime. Second, a pulser line may be employed, the turnoff resulting from the discharge of the line. Third, electrode structures may be employed that allow for optical shunting of the switch on the microstrip side of the substrate.

To examine the first possibility, we constructed stripline switches in ordinary line pulser configurations, as shown in Fig. 10. Chromium-doped, semi-insulating ($\rho \approx 10^6 \Omega$-cm) GaAs slabs were used as switching elements. A piece of alumina or G-10 was used as an insulator. In this configuration, the voltage across the load is

$$V_c = V_0 \left[\frac{Z_0}{2Z_0 + R_2} \right] \tag{12}$$

where R_s is the resistance of the switch, V_0 the applied bias, and Z_0 the load impedance. Illuminating with a 10-μJ green pulse yields a carrier denisty of 0.25×10^{20} cm^{-3} and a voltage of $V_L = V_0/3$ for a slab of size 0.022 X 0.100 in. and optical penetration depth of 2×10^{-5} cm. The temporal characteristics of the switching are shown in Fig. 11. When the switch is illuminated with a light pulse at 0.53 μm, an electrical pulse appears across the load as expected. The duration of this electrical pulse has been measured to be 70 ps for the material used in this experiment, but it varies considerably from sample to sample [5].

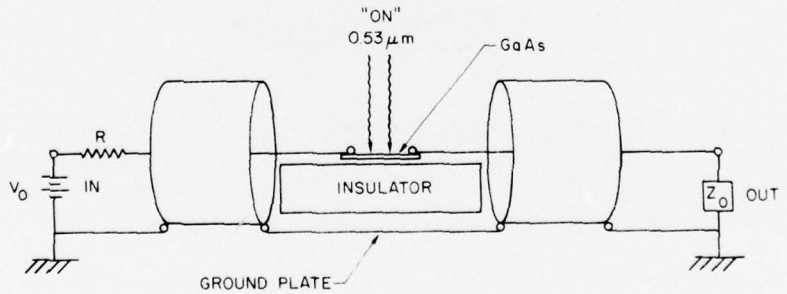

Fig 10 — Structure of the GaAs switch and the experimental setup

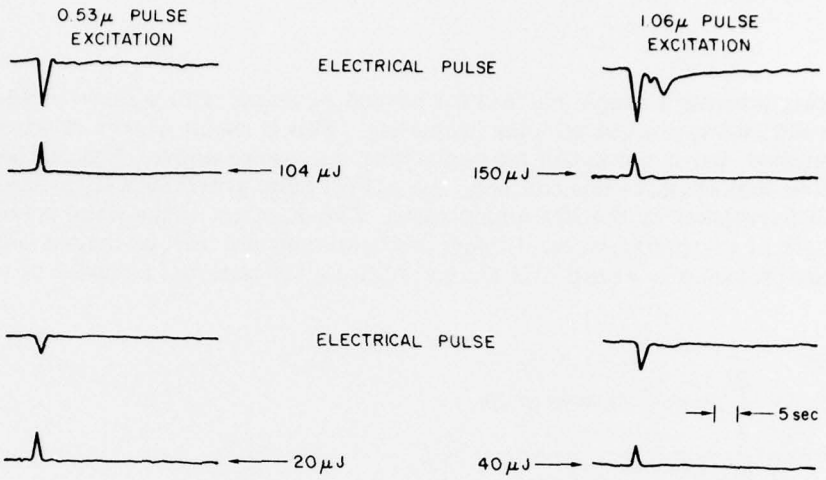

Fig. 11 — Oscilloscope traces of photo-induced electrical pulses

The relative transmission through the switch as a function of applied voltage is shown in Fig. 12. The sudden decrease in the transmission is tentatively attributed to the onset of space-charge effects. The precise mechanism is not known. This sudden dip in transmission severely limits the power-handling capability. Recently, similar configurations have been used where the duration of the pulse was of the order of 1 ns. In that case the switch was able to sustain a voltage of 8 kV across 4 mm of material and a peak transmission of 80% [6]. The possibility of optically controlled bistable switching incorporating the differential negative resistance of GaAs suggests itself, but it has not been fully explored. Chromium doping of GaAs does not substantially increase the repetition rate of the switch. Acting as a deep trap rather than a recombination center, it slowly releases charge. This implies a residual space charge, which alters the capacitance and, hence, the high-frequency performance of the device.

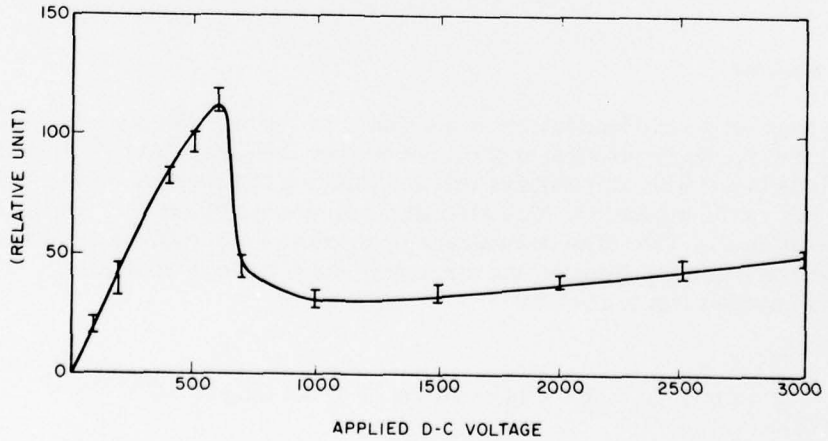

Fig. 12 — Amplitude of the "switched" electrical pulses vs applied DC voltages

Clippers

Filtering presents a simple method for generating pulses with a single pulse without relying on difficult-to-control trapping properties. This is useful when a short electrical pulse is required, but it not useful for controlling microwave power. Figure 13a shows a configuration that employs this concept. An optical pulse generates a sharp leading edge, which is differentiated by the $\lambda/4$ tuning stubs. The duration of the pulse is controlled by the length of the tuning stubs. Clipper configurations are now of limited practical use, but can provide a powerful tool for investigating the transient behavior of plasmas.

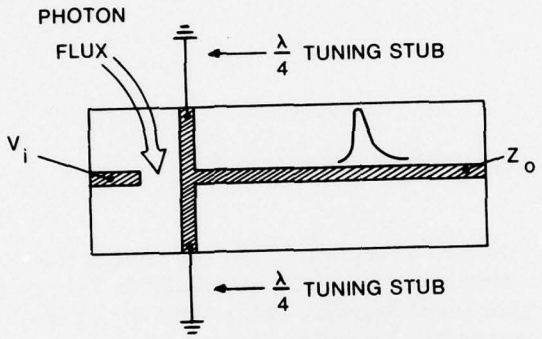

Fig. 13a — Clipper switch

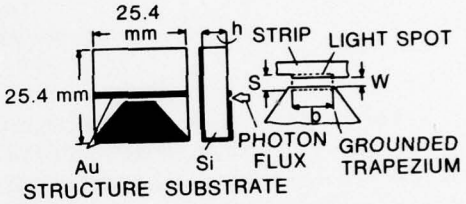

Fig. 13b — Silicon microstrip shunt modulator

Modulators

The photoconductive switch may be thought of as an optical microwave modulator. The input signal is carried in the incident optical beam, and the output signal is carried by the applied microwave bias. Switching may be thought of as a limiting case of modulation.

Shunt Modulator

The simplest form of modulator is the shunt modulator, which we have demonstrated in Figs. 1 and 8. Many practical applications require the use of light emitted at 0.9 μm from a GaAs laser. This also requires that the shunting structure be on the same side of the substrate as the microstrip. One such shunting structure used by Platte and coworkers [7] is shown in Fig. 13b. The transmission properties of the stripline are altered by injecting carriers into the gap between the microstrip and the shunting structure. In a simple model the insertion loss is given by

$$\eta = \eta_0 + \Delta\eta = \eta_0 + 20 \log (1 + 0.5\, GZ_0 \times 10^{\eta_0/20}), \qquad (13)$$

A typical result for a 50-Ω switch fabricated on a 0.55-mm silicon substrate (780 Ω-cm) with w = 0.25 mm, s = 0.3 mm, and b = 3 mm is shown in Fig. 14. To get reasonable agreement with the experiments, a reduced conductance was employed, which is given by

$$G_r = \gamma G_0 \ , \tag{14}$$

where γ is a factor attributed to shaded areas between the excited region and the conductor structures. Even if we assume a reduced electron-hole mobility of $\mu_n' + \mu_p' = 180$ cm^2 $V^{-1}S^{-1}$, it is still necessary to assume that $\gamma = 0.06$. This reduction in the overall photoconductance is more severe than that found on short time scales and points to a serious problem for these configurations.

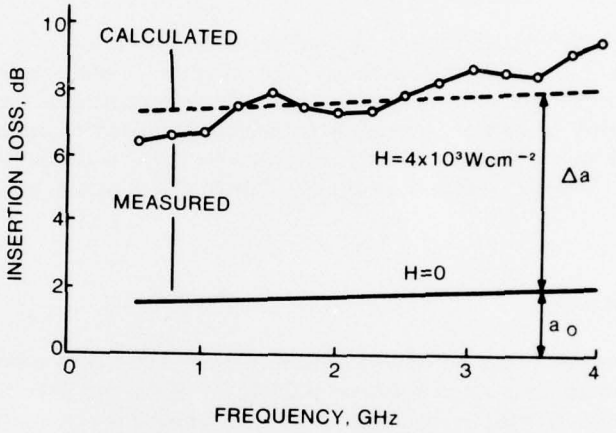

Fig. 14 — Insertion loss vs microwave frequency at minimum and maximum irradiance

The rapid sweepout of carriers in the immediate vicinity of the conducting structure generates a space charge, which limits conduction. The microwave bias can couple only capacitively to the plasma, and the overall match to ground is poor. The capacitance of a gap in a microstrip line saturates at small gap sizes [8]. Even very narrow depletion regions in the vicinity of conducting structures have relatively small capacitance, and the coupling remains small even at frequencies in the Gigahertz regime.

MODULATORS

The gap switch configuration shown in Fig. 3 also serves as a series modulator. The maximum depth of modulation m_s is given by

$$m_s = \frac{10^{\eta/20} - 10^{\delta/20}}{100} \tag{15}$$

where η is the insertion loss at maximum illumination and δ is the isolation in the dark. In the switching mode it was necessary to inject carrier densities of the order of 10^{20} cm^{-3} to achieve low insertion loss.

Auger recombination places an upper limit on the density of carriers that can be sustained over a given time interval. The rate at which carriers recombine as a result of Auger processes is given by the equation $\partial n/\partial t = -\gamma_3 n^3$. For silicon, γ_3 lies in the range of 2×10^{-31} $cm^6 s^{-1}$ and 5×10^{-30} $cm^6 s^{-1}$.

To sustain an average carrier density above 10^{19} cm^{-3} in silicon for periods in excess of 100 ns requires that the average generation rate (hence power) over the 100 ns must be equal to the average Auger recombination rate. This means that average generation rate needed to increase the density beyond 10^{19} cm^{-2} is proportional to the square density.

In Fig. 15, we have plotted the insertion loss η and isolation δ vs the gap length for a 200-μm-wide strip on a 250-μm substrate. The isloation δ was computed for a gap length of 125 μm and was extrapolated by assuming an effective capacitive area. The upper axis plots the total number of carriers necessary to achieve 0.04 Ω^{-1} conductance. These results were obtained with CW argon laser irradiation on the gap of the switch, which had an AC bias of 1 GHz. Similar results were obtained with CW krypton laser irradiation on small-gap switches.

Fundamental Parameters

To evaluate the performance of our switch, we use Eq. (5) to compute conductance and compare it with the measured value of 0.04 Ω^{-1}. Since we have to know the surface carrier mobilities of our switches to compute G_1, an experiment using a time-of-flight technique [9] in the space-charge-limited (SCL) regime was carried out to determine the carrier drift velocities from which the mobilities were obtained. The experiment is shown in Fig. 16a. The general principles of the technique are illustrated in the simple equations

$$T = \ell / V_d \tag{16}$$

and

$$\mu = V_d / E \, , \tag{17}$$

where T is the transit time of optically generated carriers traversing across a gap of length ℓ, V_d is thus the carrier drift velocity, E is the electric field across the gap, and μ is the carrier mobility we are interested in. Pairs of electron holes are created near the positive or negative electrode by ionizing radiation (frequency-doubled, mode-locked Nd:YAG) in a period much shorter than the time required for the carriers to traverse the gap. The motion of both carrier types can be observed separately either by reversing the polarity of the applied voltage or by directing the ionizing radiation on the other electrode. If the pairs of electron holes are created in a sheet that is thin compared to the spacing between electrodes (gap), and if the intensity of radiation is sufficiently low, the signal observed due to the motion of carriers should be free from space-charge effects on a

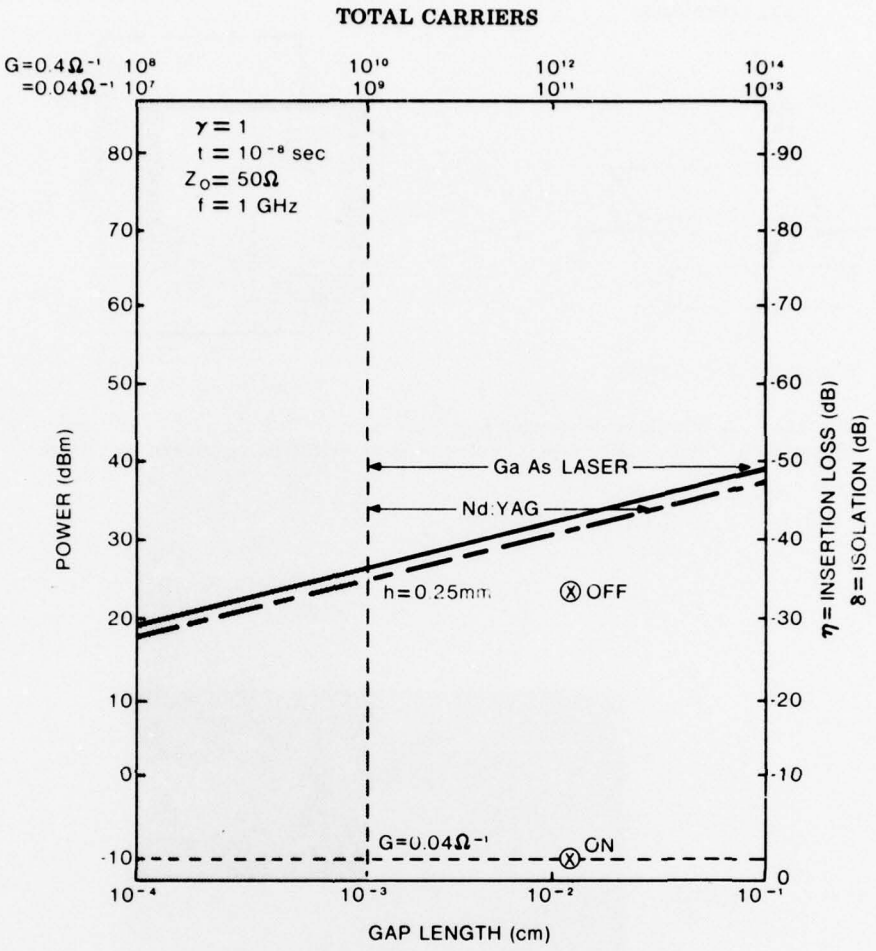

Fig. 15 — Isolation and insertion loss vs gap length

sample with a totally depleted gap. The result of our preliminary measurement of carrier mobilities is shown in Fig. 16b. We were working in the SCL regime and obtained a carrier mobility of about 160 $cm^2V^{-1}S^{-1}$ ($T = 10^{-7}$ s, $\ell = 400\ \mu$, $E = 10^3 V\ cm^{-1}$). More detailed measurements of carrier mobility are being made.

Conductance of 0.04 Ω^{-1} corresponds to an insertion loss of -2 dB for the switch with the 125-μm gap. The computed carrier lifetime is within a factor of two of the measured values, which is about 10^{-5} s. For a carrier mobility of 160 $cm^2V^{-1}S^{-1}$, the computed conductance is about 0.08 Ω^{-1}. The factor γ, as defined in Eq. (14), comes out to be about 0.5. Hence, it is necessary to employ a reduced conductance to get reasonable agreement with the experiment. For the carrier lifetime and mobility given above, the total number of carriers generated is about 10^{11} (or $10^{19} cm^{-3}$ for an irradiation

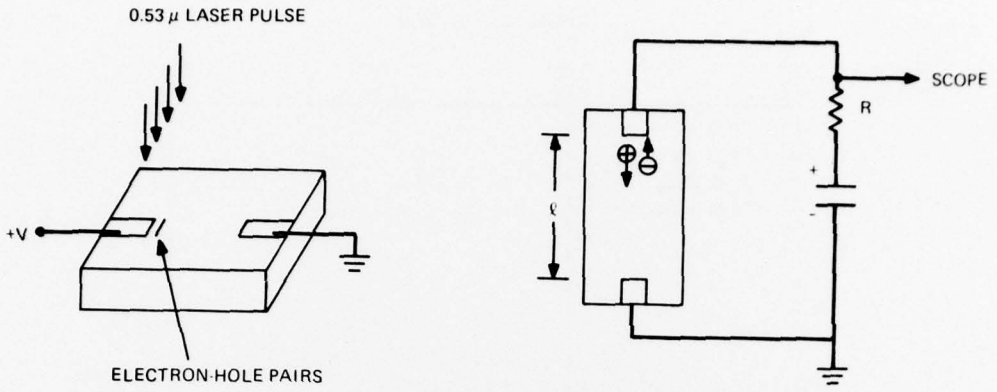

Fig. 16a — A thin sheet of electron-hole pairs is created on the surface of a piece of silicon by a 100-ps, 0.53-μm pulse near the anode with the gap biased to voltage V.

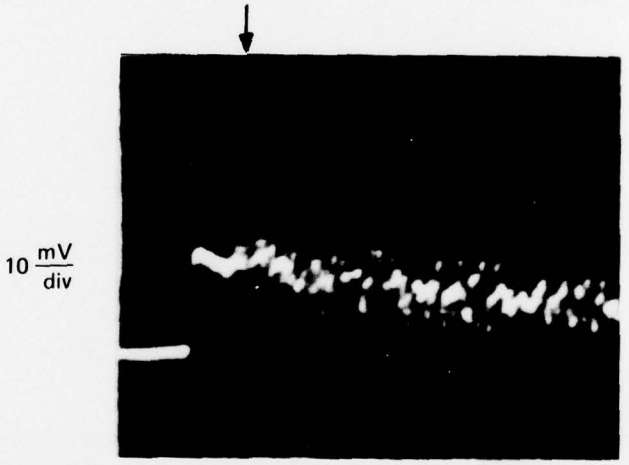

Fig. 16b — Space-charge-limited current waveform due to motion of holes. The spikes at the trailing end of the signal are due to noise.

volume of 10^{-3} cm^{-3}). This carrier concentration is at the Auger limit where the Auger lifetime is less than the monomolecular lifetime. This implies that a laser power must be quadrupled for each doubling of the carrier density. The 2-dB insertion loss is then the lowest practical limit for operation with a semiconductor laser.

The observed isolation is lower than the computed value. The most likely cause for this is the ambiguity in the gap dimension introduced by tapering the electrodes into the gap. If the effective gap length is smaller than the value used to compute the isolation, the measured isolation would be smaller, since it is proportional to ℓ. For a switch with a bigger gap, the effect of the tapering electrodes on the gap dimension would be reduced and much better isolation could be achieved. The deviation of the computed and experimental values could also be due to the breakdown in the model used to compute the gap capacitance at the reduced gap dimensions.

It is not exactly clear what caused the reduced isolation, but it appears that we are close to the limit on the performance of the switch with CW laser irradiation. Our excitation levels are consistent with the limit imposed by Auger processes. The shadow factor of $\gamma = 0.5$ is an order of magnitude improvement over the previous best results ($\gamma = 0.06$) [7]. This is the result of developing a method of tapering electrodes on small-gap switches that has also achieved a 10-dB reduction in insertion loss. Because the performance of the optical switch has been pushed to the limit, it seems that further improvements require new concepts.

Gain—Bandwidth Limitations

Ultimately, the performance of this approach to switching and modulation has a gain-bandwidth product limitation imposed by the photoconductivity mechanism. For DC switching, this limitation is given by the well-known relation

$$Gf_B \leqslant \frac{1}{T}\,, \tag{18}$$

where G is the usual photoconductive gain, f_B the modulation bandwidth, and T the transit time for a carrier across the photoconductor, in this case the gap length. The lower bound on T is the dielectric relaxation time of the photoconductor. The bandwidth is inversely proportional to the time spent by a carrier within the photoconductor, which is either the recombination lifetime T_f or carrier sweep-out time, whichever is shorter.

Now, the bandwidth with which we are presently concerned is not to be confused with the electrical bandwidth, which places a limit on the shortest burst of electrical energy that can be propagated down the microstrip. The Auston switch operates far from the limit imposed by Eq. (14). Both the gain and the modulation bandwidth are small. Consider the DC case, with a bias sufficient to saturate the carrier velocity within the gap, and also consider that the recombination lifetime is greater than the sweep-out time. For pulsed operation, the maximum gain, $G = 1$, is realized when the switching time equals the sweep-out time. The minimum transit time is the dielectric relaxation time of the gap, which is determined by the resistivity, and is of the order of 10^{-7} s for

reasonable isolation. The actual transit time is longer for the application because of plasma effects associated with the high density of carriers required for the low-insertion-loss state. The pulse duration time t_D controls the gain for time less than T so that the gain is given by

$$G = \frac{t_D}{T} = \frac{t_D}{10^{-7}\ \text{s}} \ . \tag{19}$$

A square electrical pulse can be obtained only for times $t_D \ll t_r$, say for example 10^{-9} s, and consequentially a current gain of 10^{-2}. This yields a maximum power gain of 10^{-4} if the power of the injection pulse (optical) is averaged over the duration of the electrical pulse. In this case, a 10-μJ optical pulse yielding an average power of 10^3 W will at best create a 0.1-W electrical pulse of 1-ns duration. Furthermore, obtaining a square pulse requires that the optical pulse duration equal the rise time, which in the present case is of the order of 10 ps, increasing the injection power by two orders of magnitude so that the instantaneous power gain G_{PI} is of the order of 10^{-6}. The bandwidth of the electrical pulse is limited by the duration of the optical pulse. Thus, to use the Auston switch at its maximum instantaneous bandwidth to generate 10^{-11} s electrical pulses, the current gain is 10^{-4} and the power gain 10^{-8}. The modulation bandwidth remains unchanged and is on the order to 10^7 s. This illustrates the principal tradeoff for the Auston switch — small gain and small modulation bandwidth for large instantaneous bandwidths. Introducing fast recombination centers, such as gold in silicon, could ideally increase the modulation bandwidth, to equal, in some instances, the instantaneous bandwidth. But as was experienced in chromium-doped GaAs, this occurs only if recombination, not trapping, occurs at the chromium site. According to Eq. (18), gains much greater than unity can be achieved if the carrier photoconductive lifetime is greater than the transit time. This can be accomplished in several ways, one of which is to apply an AC bias on carriers equivalent in our case to the microwave signal we wish to control so that the period of oscillation is approximately equal to the transit time. Another way is to make the contact recombination velocity as small as possible (non-ohmic); then we may replace the transit time by the period of oscillation, the bandwidth being the inverse of the bulk carrier recombination lifetime, or

$$G \leqq \frac{f_m}{f_b} = \frac{T_r}{t_m} \ . \tag{20}$$

Thus, to achieve a given gain for a given modulation bandwidth, we must employ a higher bias frequency. Associated with this are correspondingly smaller gaps and hence reduced isolation and signal power. This approach was employed in achieving the Auger limit of gain for the gap modulator. Further improvement in the gain can be achieved, at the expense of overall bandwidth, by incorporating impedance transformations. Sommers [10] has investigated the limits of this approach from the photodetection point of view. Utilizing a re-entrant cavity for obtaining impedance match results in the expression for gain

$$G \leqq \frac{f_m}{f_b} Q, \tag{21}$$

where Q is the overall quality factor of the cavity plus coupling.

For a shunting modulator with a $\lambda/4$ resonant transformation, the magnitude of the transmission is given by [11]

$$T = \frac{\left|1 - q^2 Z_0 G\right|}{1 + q^2 Z_0 G} , \tag{22}$$

where q is the impedance ratio. It follows then that the photoconductivity necessary for 100% modulation is reduced by the factor $1/q^2$, as is the modulation bandwidth according to Eq. (21).

CONCLUSIONS

The limitations of optically gating short bursts of electromagnetic radiation in the gigahertz regime can be satisfactorily established within the framework of simple photoconductivity principles. This is most compactly expressed in the form of a gain—bandwidth product limitation. The overall efficiency of a given device may be evaluated by how well its performance approaches this limit. From this point of view, Auston's original microstrip gap switch is an inherently inefficient approach, since it achieves a high instantaneous bandwidth by truncating the photoconductive gain without a comensurate increase in the modulation bandwidth. Introducing deep traps does not improve the efficiency, but replaces optically controlled truncation of photoconductivity with trap-controlled truncation.

Optical modulators with efficiencies approaching the theoretical limit have been fabricated by adjusting the dimension of the gap so that the optically injected carriers are not swept out within a period of the microwave bias.

Additional gain can be achieved by providing impedance-matching structures. In this mode, optical microstrip modulators could be effectively operated with the use of commercially available semiconductor diode lasers.

Finally, the generation or control of short bursts of relatively high-powered microwave radiation by relatively low-power optical injection of carriers into a lumped semiconductor element runs contrary to the underlying principles of simple photoconductivity. Circumventing the fundamental gain—bandwidth product limitation intrinsic to conventional photoconductivity will require more sophisticated devices, such as distributed modulation and/or a physical mechanism (i.e. carrier avalanche), that go beyond simple lumped-element photoconductivity.

REFERENCES

1. D. H. Auston, Appl. Phys. Lett. **26**, 101 (1975).
2. M. V. Schneider, Bell Syst. Tech. J. **48**, 1421 (1969).
3. R. W. Beatty and D. M. Kerns, Proc. IEEE **52**, 84 (1964).
4. A. M. Johnson and D. H. Auston, IEEE Trans. **QE-11**, 283 (1975).
5. C. H. Lee, Appl. Phys. Lett. **30**, 84 (1977).

6. A. Merriaux, private communications, University of Rochester, Laboratory for Laser Fusion, 1978.
7. W. Platte and G. Appelhans, Electron. Lett. **12**, 270 (1976).
8. Y. Rahmat-Samii, T. Itoh, and R. Mittra, IEEE Trans. **MTT-22**, 372 (1974).
9, M. Martini, J. W. Mayer, and K. R. Zanis, Appl. Solid State Sci. **3**, 181 (1972).
10. H. S. Sommers, Jr., and W. B. Teutsch, IEEE Proc. **52**, 144 (1964).
11. V. W. Platte, Nachrichtentechn. Z. **29**, 737 (1976).
12. M.A. Lampert, and P. Mark, *Current Injection in Solids*, Academic Press, New York (1970).
13. N. F. Mott and R. W. Gurney, *Electronic Processes in Ionic Crystals*, 2nd ed., Clarendon Press, Oxford (1948).

Appendix
THE MICROSTRIP SWITCH CHARACTERISTICS

The material used to fabricate our opto-electronic switches was high-resistivity π-silicon purchased from Wacker-Chemitronic. The specific device shown in Fig. A1 consisted of a silicon slab of resistivity $\rho = 3 \times 10^4 \Omega$-cm and cut in $<111>$ orientation, which was chemically polished on both faces. The silicon slab was etched for 1 to 2 min in 6:1:1 mixture of deionized water, nitric acid, and hydrofluoric acid. The etched silicon was rinsed in deionized water. Metallic contacts were evaporated onto the slab immediately after the etching process. The microstrip conductors were formed by evaporating 5000 Å of aluminum through a shadow mask. This was followed by a heat treatment of 10 min in flowing nitrogen and hydrogen (15% H_2 and 85% N_2). The microstrip was connected to BNC connectors through OSM launchers. Silver paste was used to make electrical contacts for the launchers and the aluminum electrodes.

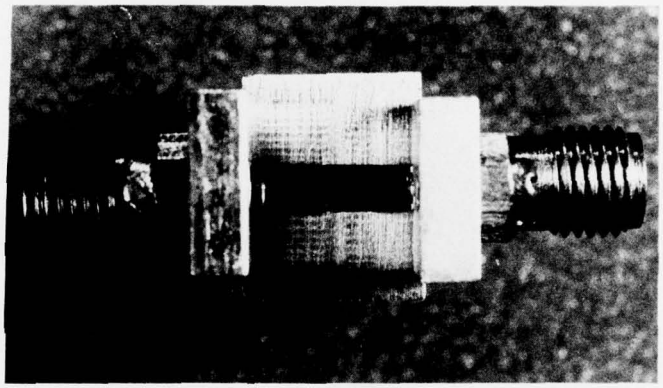

Fig. A1 — Silicon switch with a 30-mil gap mounted on an aluminum block

A switch so fabricated had a $p^+ \pi p^+$ structure. The current—voltage (I—V) characteristics of the switch were checked in the dark using a Tektronix 575 Transistor-curve Tracer. This check served two purposes: (a) to make sure that the microstrip conductors were making contact with the outside world, and (b) to find out whether ohmic contact had been made between Si and Al. Fig. A2a shows the I—V characteristics of the gap of a switch, and Fig. A2b shows the I—V characteristics on a log-log plot.

We note from the log-log plot that the slope changed from 1 to 2 at V_x. This suggests that for bias voltages smaller than V_x, $I \propto V$, and for voltages larger than V_x, $I \propto V^2$. The slope 1 region corresponds to Ohm's law and the slope 2 region is the space-charge-limited (SCL) current regime.

As shown in Fig. A3, the I—V characteristics of the gap of another switch showed a somewhat different behavior. The slope was 2 all the way through between the two limits of the Tektronix 575 scope. This showed that the switch was already in the SCL current

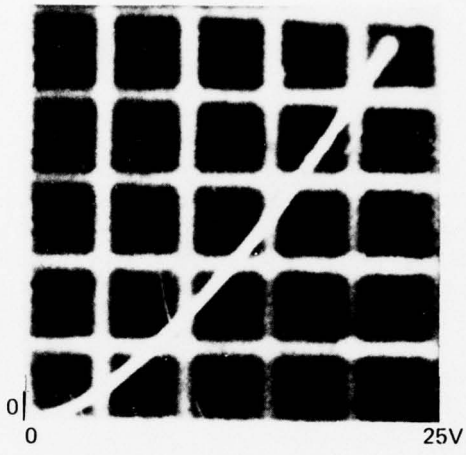

(a)

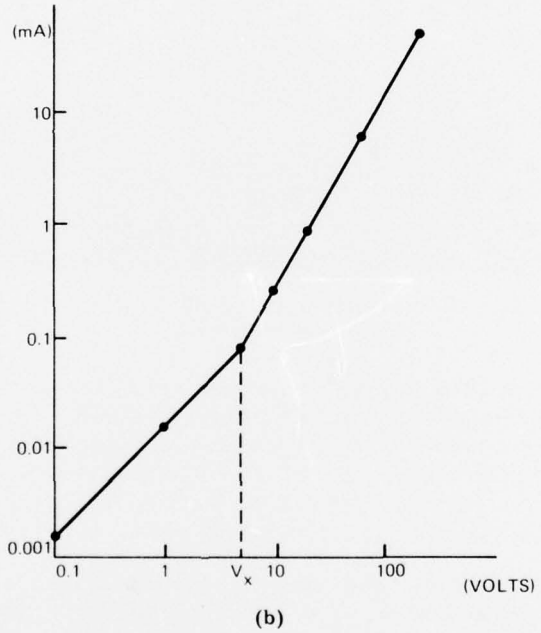

(b)

Fig. A2 — Forward-current characteristics of the gap of a switch. The gap length is 5 mils.

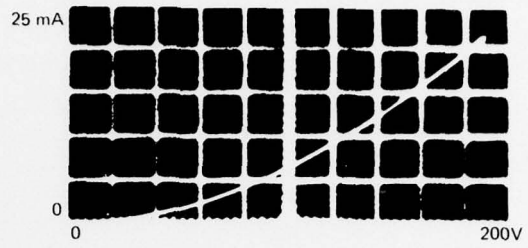

(a)

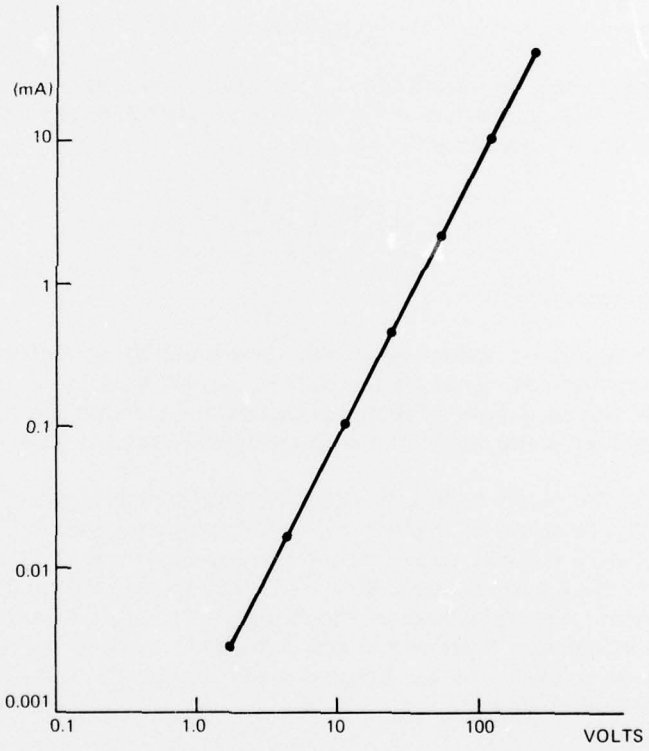

(b)

Fig. A3 — Forward-current characteristics of the gap of a switch. The gap length is 30 mils.

regime even at very, very low bias voltages. This is the same as saying that the concentration of shallow traps in this switch was lower than in the other switch. (This point will be elaborated in the next paragraph.) Since both switches were made of the same material, different behaviors of the I—V characteristics seemed to come from the fabrication processes. Although we had tried to maintain the same fabrication conditions for every switch, the difference in I—V characteristics suggested that different shallow trap concentrations were introduced into the silicon during different fabrications.

A hole trap at E_t is said to be shallow if the Fermi level F lies above E_t and if $[(F\text{-}E_t)/kT] > 1$. When the switch is biased by low voltages, we expect that Ohm's law will be observed. Although at any voltage, however small, there will be excess charge injected into the silicon from the aluminum-silicon contact, there cannot be significant departures from Ohm's law until the average, injected, excess, free-hole concentration becomes comparable to the concentration of shallow hole traps. Thus the crossover from Ohm's law to the square law, that is, the onset of SCL current injection, takes place at the voltage V_x given by

$$V_x \approx ep_t L^2/\epsilon_r\epsilon_0 \tag{A1}$$

where p_t is the trapped-hole concentration, L is the gap length, and ϵ_r is the dielectric constant.* The current—voltage relationship in the SCL current injection regime is given by the Mott—Gurney law† for one carrier injection as

$$J = \frac{9\epsilon_r\epsilon_0\mu_h V^2}{8L^3} \tag{A2}$$

where μ_h is the hole mobility.

When a switch having an ohmic region was illuminated by moderately intense room light, the current increased as shown by the shift in current level in Fig. A4. However, for the SCL switch, the same level of illumination did not increase the current flow at all. Thus, photosensitization is also associated with switches possessing ohmic characteristics.

For a switch in the ohmic region, the injected charge concentration was very low compared to the concentration of shallow traps. Light illumination created pairs of electron holes in the silicon in a way as to increase the doping of the silicon. Hence the resistance decreased and more current could flow. The illumination also increased V_x and decreased the dielectric relaxation time of the switch. For a switch in the SCL regime, light-injected pairs of electron holes would not increase the current because the total charge the device could hold is limited by the injected space charge. So, there are no additional charges to increase current flow.

It is convenient to define the effective drift mobility μ_h. If the free-hole concentration is disturbed from its thermal equilibrium value p_0, say by injection, to a new value p, then on a time scale long compared to the microscope trapping and detrapping times,

---

*M. A. Lampert, *Injection Currents in Solids*, Academic Press, New York, 1965.
†N. F. Mott and R. W. Gurney, *Electronic Processes in Ionic Crystals*, Clarendon Press, Oxford, 1940.

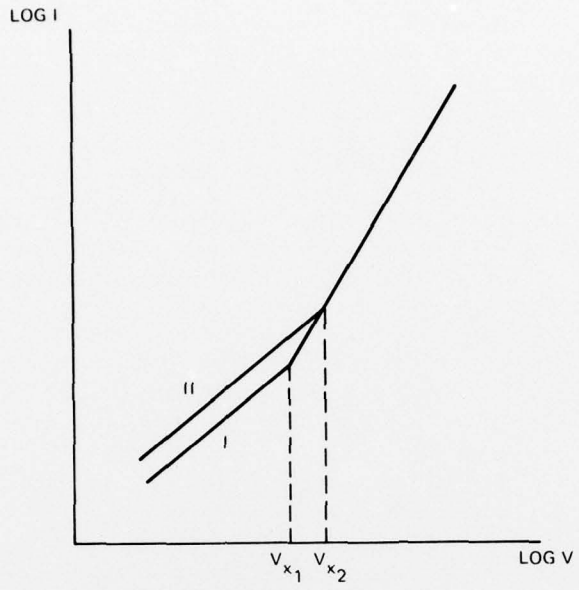

Fig. A4 — Curve I is the current level at dark and Curve II is the new current level of a switch with light illumination.

the population p_t of the hole traps will be in quasi-thermal equilibrium with p. Then the entire body of injected holes, $p + p_t \approx p_t$, will have the effective drift mobility $\mu_h = (p/p_t)\mu$. In terms of μ_h, Eq. (A1) is equivalent to $t_{x,h} \approx t_r$, with

$$t_{x,h} = \frac{L^2}{t_r(\mu_h V_x)} = \frac{\epsilon_r t_0}{e p_0 \mu}$$

and

$$\mu_h = \left(\frac{p}{p_t}\right)\mu,$$

where $t_{x,h}$ is the effective transit time, between cathode and anode, of the entire body of injected charge at voltage V_x.